Experimental Thermal and Fluid Science 35 (2011) 660–669

Contents lists available at ScienceDirect

Experimental Thermal and Fluid Science

journal homepage: www.elsevier.com/locate/etfs

Experimental investigation of the performance of a thermoelectric generator based on Peltier cells

G. Casano *, S. Piva

ENDIF, ENgineering Department In Ferrara, Università di Ferrara, via Saragat 1, Ferrara 44122, Italy

ARTICLE INFO

Article history:
Received 16 July 2010
Received in revised form 24 December 2010
Accepted 26 December 2010
Available online 31 December 2010

Keywords:
Thermoelectric conversion
Thermoelectric modules
Power generation

ABSTRACT

An experimental investigation is carried out to characterize the performance of thermoelectric modules used for electric power generation over a range of different resistance loads. The performance of a Peltier cell used as a thermoelectric generator is evaluated in terms of power output and conversion efficiency. The results show that a thermoelectric module is a promising device for waste heat recovery.

1. Introduction

Thermoelectric conversion may be defined as the result of a process by which heat is converted into electricity through the use of a heat-to-electricity conversion device. Thermoelectric conversion, besides occurring in simple thermocouples, forms the basis of reversible thermoelectric modules (TEMs), which can work either as coolers when supplied with electricity, or as generators when supplied with heat.

A TEM consists of alternate ingot-shaped n- and p-type semiconductor thermoelements, which are connected electrically in series with metal connecting strips, sandwiched between two electrically insulating but thermally conducting ceramic plates [1].

The utilization (generator or cooler) determines the temperature under which the thermoelements operate, and hence the choice of materials for the thermoelements. For low temperature applications (commonly coolers) BiTe alloys are used; in contrast high temperature materials such as PbTe or SiGe alloys, are used in thermoelectric generators [2]. However, the BiTe alloys used in conventional coolers have recently become relatively cheap, suggesting their use also in thermoelectric generators [3].

Recent review papers (Riffat and Ma [4], Bell [5], Kajikwa [6], and for the automotive sector Vázquez et al. [7]) summarize the potential applications in power generation of thermoelectric devices. These works make it evident that recent advances in materials and material processing have led to higher theoretical thermoelectric conversion efficiencies. However, when using TEMs in the power generation mode the final thermal efficiency is limited also by other factors: the reduction of the heat losses, the design optimization to reduce the parasitic losses and the appropriate choice of materials.

In the literature only a limited number of papers are available dealing with the thermal experimental performance of a thermoelectric generator. Some authors investigate directly the performance of TEMs. Leavitt et al. [8] discuss the critical requirements for accurate testing of a TEM and Takazawa et al. [9] report the design and development of a testing system for TEMs operating at high temperature. Rauscher et al. [10] present an apparatus for measuring the conversion efficiency and other key properties of TEMs; experimental data for a high efficiency Bi_2Te_3 module are discussed and compared with the results obtained from a theoretical model. From their experimental data Sandoz-Rosado and Stevens [11] analyze a TEM under a wide range of temperature and loading conditions. Their attention focused on the measurement of the heat flow into the module and the parasitic losses inside the TEM. Gou et al. [12] study experimentally a low-temperature waste heat thermoelectric generator. The data are used for the validation of the model used to guide the analysis and the optimization of the generator.

Other authors carry out direct investigations on specific applications of TEMs. Crane and Jackson [13] study the behaviour of a thermoelectric generator heated by a hot liquid flow and cooled by an air stream. Saqr et al. [14] report the application of an exhaust-based thermoelectric generator in the thermal design of an automobile. For three different examples they obtained data for the overall efficiency, the temperature difference across the TEMs

* Corresponding author. Address: ENDIF, via Saragat 1, 44122 Ferrara, Italy. Tel.: +39 0532 974890; fax: +39 0532 974870.
E-mail address: giovanni.casano@unife.it (G. Casano).

0894-1777/$ - see front matter © 2010 Elsevier Inc. All rights reserved.
doi:10.1016/j.expthermflusci.2010.12.016

Nomenclature

A	cross area of the thermoelement (mm^2)
I	electric current (A)
L	length (mm)
K	thermal conductance ($W K^{-1}$)
m	number of modules in the generator
N	number of thermocouples per module
P	electric power output on the load resistance (W)
Q	heat power (W)
R	electric resistance (Ω)
T	temperature (K)
V	electric voltage (V)
Z	figure of merit ($\alpha^2/\rho\lambda$) (K^{-1})

Subscripts

A	air
b	bolts
CC	closed circuit
C	cold junction
cer	ceramic insulator
env	environment
g	thermal grease
gen	thermoelectric generator
H	hot junction
In	input
ins	insulation
J	Joule heater
L	resistance load
n	n-type semiconductor
ov	overall
p	p-type semiconductor
TEM	thermo electric module
OC	open circuit
s	stainless steel

Greek symbols

α	Seebeck coefficient ($V K^{-1}$)
Δ	difference
λ	thermal conductivity ($W m^{-1} K^{-1}$)
ρ	electrical resistivity (Ω m)
ε	conversion efficiency

and the conversion efficiency. Niu et al. [15] carry out an experimental study of a thermoelectric conversion unit, consisting of commercially available TEMs incorporated in a parallel plate heat exchanger.

In the process of reduction of the direct experimental data, it is necessary to use a mathematical model of greater or less simplification. Such a model involves the electrical and thermal properties of the TEM, and often these are unknown. Interesting procedures have been recently developed to obtain these properties from manufacturers' data (Luo [16] and Palacios et al. [17]). These are preferable to the situation where the experimental data themselves are used to determine the parameters [13].

The present paper reports an experimental investigation of the performance of a power generation device in which we have used multiple Peltier modules in the Seebeck mode. The thermoelectric generator is analyzed on the basis of the experimental data for the 'open' and 'closed' circuit voltage, electric power output and conversion efficiency as a function of the temperature. In the laboratory a Joule resistor is used as the thermal source instead of waste heat. The experimental data give significant information about the behaviour of the thermoelectric generator. In particular the effects of practical but unavoidable details are evidenced, such as the clamping of bolts and the fitting of thermal insulation between TEMs.

2. Experimental apparatus

A schematic diagram of the test section is shown in Fig. 1. The test section consists of a thermoelectric generator made of nine TEMs ($40 \times 40 \times 3.8$ mm) connected electrically in series. They are sandwiched between a square plate of aluminium ($200 \times 200 \times 4$ mm) and a conventional heat sink of the same area. Uniform pressure is ensured by using 22 stainless steel screws (2.5 mm nominal diameter, $\lambda_s = 16\ W m^{-1} K^{-1}$) to clamp the assembly together. Uniform contact between the Peltier cells and the aluminium plates is enhanced by a thin layer of thermal grease (SG500, $\lambda_g = 0.77\ W m^{-1} K^{-1}$). Thermal insulation comprised of cellular rubber is placed between the modules.

The overall dimensions of the aluminium heat sink are 200 mm by 39.2 mm by 200 mm for the width, height and length respectively. The finned surface consists of 20 fins with thickness 3.2 mm and height 30.8 mm. The gap between the fins is 7.2 mm. To facilitate heat release by the thermoelectric generator, the fins of the bottom plate are immersed in a bath, where water flows at room temperature (Photo 1).

The hydraulic circuit is schematically shown in Fig. 2. It is of the 'open' type, that is with constant head feeding and receiving tanks open to the atmosphere. The former feeds the heat transfer section. After passing this section, the fluid is collected into the receiving tank, from where it is pumped up to the feeding tank. The operating fluid is cooled through the pipe walls by heat transfer with the surrounding air.

The measured flow rate of the water is $7.2 \times 10^{-5}\ m^3\ s^{-1}$. In the gap between the fins the Reynolds number is 272. The overall thermal resistance of the heat sink, based on the experimental data, is 0.0152 ± 0.0015 K/W. An estimation of the overall thermal

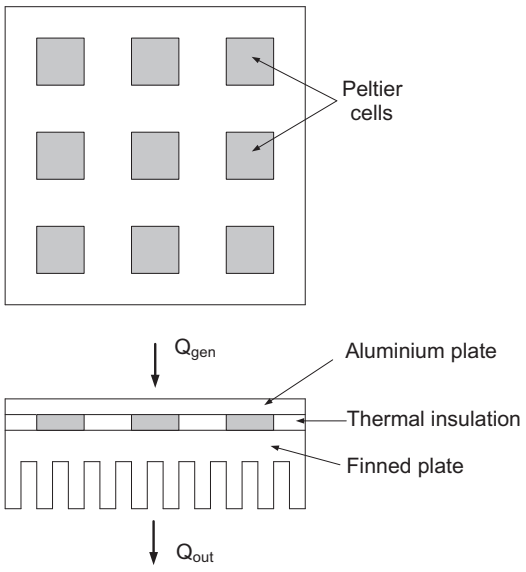

Fig. 1. Schematic diagram of the test section.

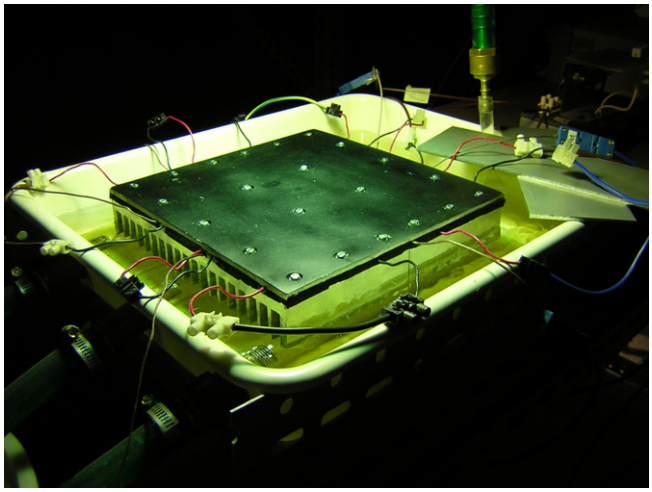

Photo 1. Thermoelectric generator in a small experimental bath.

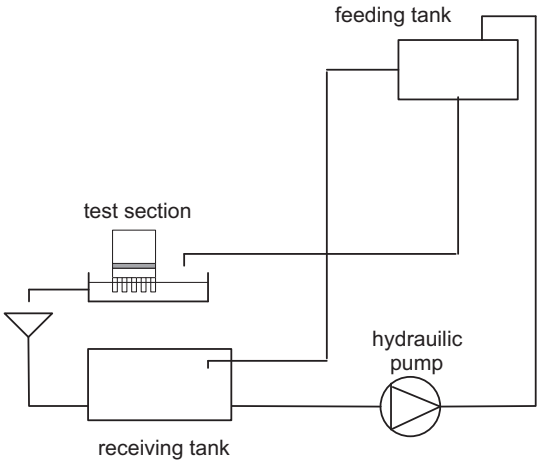

Fig. 2. Schematic overview of the heat transfer system.

resistance of the heat sink, based on the results of Morini [18], gives 0.0148 K/W, in very good accordance.

A heat flow is supplied to the top surface of the thermoelectric generator. It is obtained by dissipating via the Joule effect an assigned power in a nickel-chrome resistor. This resistor of square shape and of the same dimensions as the outside top surface of the thermoelectric generator, is placed under a layer of insulating material (mineral wool near the heater, glass wool near outside). The total thickness of the layers of insulating material is 200 mm and the thermal conductivity is 0.03 $W\,m^{-1}\,K^{-1}$. The insulating layer is confined sideways by a 40 mm thick layer of expanded polyurethane.

In Table 1 are reported the remaining geometrical parameters of the generator.

The temperature on the surface of the modules is measured using copper-constantan thermocouples. Three thermocouples are placed on the aluminium finned plate in the space between the modules. Nine thermocouples are fixed on the top plate over the modules. Two armored thermocouples of type K are placed inside the duct feeding the bath and in the air, respectively.

The fourteen thermocouples are connected to an acquisition data system Agilent 34970A. The same instrument is used for the measurement of the circuit voltage on the resistance load. When more thermocouples are placed on a surface, the average value of the data is considered.

Table 1
Geometrical parameters of the generator.

Data	Symbol	Value	Unit
Cellular rubber thickness	L_{ins}	4.3	mm
Hot side thermal grease thickness	L_{gH}	0.5	mm
Cold side thermal grease thickness	L_{gC}	0.2	mm
Diameter of the bolts	D_b	2.5	mm
Average thickness of the heater	L_{heater}	7	mm
Area of the heater	A_{heater}	0.04	m^2

The electric resistance of the Joule heater has been measured for different values of the temperature. A variation law of this electrical resistance is obtained by means of a linear interpolation. The knowledge of the dependency of the electric resistance on the temperature allows the monitoring of the electric power supplied by means of simple measurements of voltage.

3. System modelling

In order to predict the performance of the thermoelectric generator as a function of the experimental thermal conditions, a lumped parameter model has been formulated. The electrical scheme of the model is shown in Fig. 3. In Fig. 4 a section of a thermoelectric module is shown.

The theoretical model gives the values of the main parameters, expressed in terms of the temperature difference established by the heat flow.

Each pair of thermoelements (Fig. 4) produces an electromotive force by the Seebeck effect given by:

$$V'_{OC} = (\alpha_p - \alpha_n)(T'_H - T'_C) \quad (1)$$

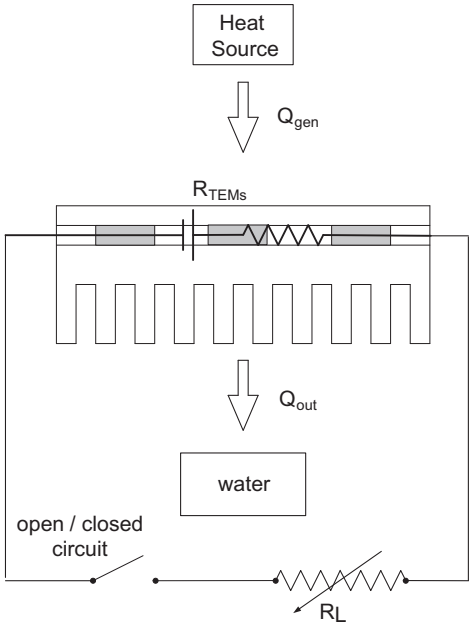

Fig. 3. Electrical scheme.

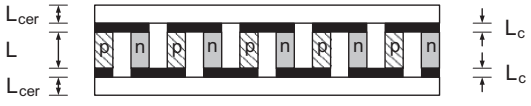

Fig. 4. Thermoelectric module section.

The top and bottom temperatures, T'_H and T'_C respectively, are at the hot and cold junctions of the thermoelements; α_p and α_n are the Seebeck coefficients of the p- and n-type semiconductors, respectively.

When a resistance load is inserted, the power production starts. The 'closed' circuit voltage, V_{CC}, at the ends of the resistance load, R_L, is given by:

$$V_{CC} = \frac{R_L}{R_{TEM} + R_L} mN(\alpha_p - \alpha_n)(T'_H - T'_C) \tag{2}$$

where the electromotive force is extended to the number of thermocouples per module, N, and the number of modules, m. R_{TEM} is the internal resistance of the thermoelectric generator, calculated as the sum of the electric resistance of each thermoelement pair, extended as above to the numbers N and m, where the electric resistance per thermoelement pair is given by the sum of the electric resistance of two p- and n-type thermoelements:

$$R' = \rho_n \frac{L_n}{A_n} + \rho_p \frac{L_p}{A_p} \tag{3}$$

In Eq. (3) A_p, L_p, ρ_p and A_n, L_n, ρ_n indicate the cross sectional area, the length and the electrical resistivity of the p- and n-type thermoelements, respectively.

The power output dissipated by the resistance load is given by:

$$P = \frac{R_L}{(R_{TEM} + R_L)^2} \left[mN(\alpha_p - \alpha_n)(T'_H - T'_C) \right]^2 \tag{4}$$

The heat input, Q_{in}, for the pair of thermoelements for steady operations, is composed of three terms due to heat conduction, and the Peltier and Joule effects. This heat flow is given by:

$$Q_{in} = K'\Delta T' + (\alpha_p - \alpha_n) T'_H I - \frac{1}{2} R' I^2 \tag{5}$$

where K' is the thermal conductance of a thermoelement pair, given by:

$$K' = \left(\lambda_p \frac{A_p}{L_p} + \lambda_n \frac{A_n}{L_n} \right) \tag{6}$$

In Eq. (6) A_p, λ_p and A_n, λ_n indicate the cross sectional area and the thermal conductivity of the p- and n-type thermoelements, respectively.

The heat input into the thermoelectric modules is given by:

$$Q_{TEM} = mNQ_{in} \tag{7}$$

where N and m are as defined above.

The electric current, I, in Eq. (5) is that circulating in the generator when the load is inserted, given by:

$$I = \frac{mN(\alpha_p - \alpha_n)(T'_H - T'_C)}{R_{TEM} + R_L} \tag{8}$$

The thermoelements are sandwiched between two ceramic plates (Fig. 4) in thermal contact with the assembly surfaces through thin layers of thermal grease. The temperature is measured on the assembly surfaces, firstly in the immediate proximity of the TEM on the bottom, and also on the top plate over the modules on the top. Then, to obtain the values of temperature inside the ceramic plates at the hot and cold junctions, the theoretical model proposed by Chen et al. [19] is used. This mathematical model is based on a thermal balance for the TEM and its connecting structure. For the closed circuit the temperature difference over the junctions $(T'_H - T'_C)$ is a function of that outside the ceramic plates $(T_H - T_C)$ and other parameters:

$$(T'_H - T'_C) = (T_H - T_C) f(R_L, K_h, K_c) \tag{9}$$

where R_L is the resistance load, K_h, K_c are the upstream and downstream thermal conductance of the hot and cold junction of the pair of thermoelements, respectively.

When the circulating current, I, tends to zero, the relationship between $\Delta T'$ and ΔT becomes (Rowe [20]):

$$T'_H - T'_C = \frac{T_H - T_C}{\left(1 + \frac{K'}{K_h} + \frac{K'}{K_c}\right)} \tag{10}$$

In this case for each thermoelement pair the voltage of the model tends to the 'open' circuit voltage and is obtained as:

$$V'_{OC} = (\alpha_p - \alpha_n) \frac{(T_H - T_C)}{\left(1 + \frac{K'}{K_h} + \frac{K'}{K_c}\right)} \tag{11}$$

For the generator as a whole, and using the data from all the pairs of thermoelements, the 'open' circuit voltage V_{OC} is given by:

$$V_{OC} = mNV'_{OC} \tag{12}$$

4. Experimental tests

Each measurement was carried out with the load in ('closed' circuit) and then repeated with the load out ('open' circuit). To start any test series the resistance load is connected. The test continues with the insertion of the hydraulic pump to circulate the water in the cooling system. Successively, the Joule heater is supplied to give the assigned power input. The monitoring of the test determines when steady state conditions have been attained, which is when the data acquisition is started. All the parameters are then sampled every 150 s, over a period of 40 min.

When the data acquisition is finished for the 'closed' circuit, the resistance load is disconnected and the procedure is repeated for the 'open' circuit.

The useful power dissipated by the resistance load, R_L, is calculated on the basis of the electric measurements using the following equation:

$$P = \frac{V_{CC}^2}{R_L} \tag{13}$$

where V_{CC} is the 'closed' circuit voltage over the resistance load.

In order to obtain the efficiency of the generator this useful power has to be compared with the heat flow input. A lumped parameter distribution of the heat flow can be obtained with a thermal resistance scheme (Fig. 5). The overall heat power input into the generator, Q_{gen}, is the difference between the electric power supplied to the Joule heater, Q_J and the heat leakage through the insulation materials placed over the Joule heater, Q_{env}:

$$Q_{gen} = Q_J - Q_{env} \tag{14}$$

Q_{gen} is composed of two terms: the heat power input into the TEMs, Q_{TEM}, and the heat lost by conduction through the assembly structures. Consequently, the heat power into the TEMs is given by:

$$Q_{TEM} = Q_{gen} - (Q_b + Q_{ins}) \tag{15}$$

where Q_b is the heat leakage through the bolts clamping the assembly together and Q_{ins} is the heat flow through the insulating material (cellular rubber) placed between the cells.

Owing to the significant temperature difference between the plates, in the calculation of the heat losses through the insulating material a linear dependence of the thermal conductivity on temperature is adopted for the cellular rubber.

The conversion efficiency of the TEMs is given by the ratio between the measured power output, Eq. (13), and the net power into the modules, Eq. (15):

$$\varepsilon_{TEM} = \frac{P}{Q_{TEM}} \tag{16}$$

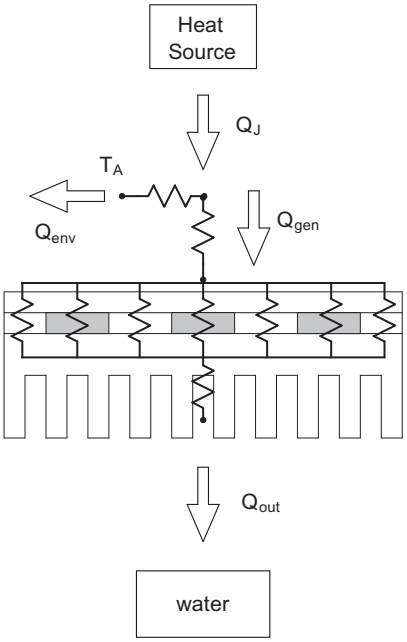

Fig. 5. Thermal scheme.

The overall conversion efficiency of the generator is given by the ratio between the measured power output, Eq. (13), and the overall power into the generator, Eq. (14):

$$\varepsilon_{gen} = \frac{P}{Q_{gen}} \tag{17}$$

5. Results and discussion

Data for the experimental performance of the generator for different operating conditions are presented.

In this experiment very cheap commercially available Peltier cells are used but the manufacturer's data sheets were unavailable. Thus the procedures proposed in [16,17] were inapplicable. Also the way of using the experimental data themselves to determine the parameters, as adopted in [13], was considered inappropriate. Since many parameters are mandatory when using the lumped parameter model for predictions, a cell was destroyed to characterize its components. These were measured using an optical microscope. Referring to Fig. 4 for the meaning of the symbols, $L = 1.6$ mm, $L_c = 0.5$ mm, $L_{cer} = 0.6$ mm; the p and n legs show the same square section with side 1.5 mm and transverse area $A = 2.25$ mm^2. Every module consists of 127 pairs of thermoelements.

With X-ray spectroscopy the chemical composition of the semiconductors was identified: $Bi_{0.5}Sb_{1.5}Te_3$ for the p-type semiconductor and Bi_2Te_3 for the n-type semiconductor.

For the remaining parameters which are needed, values are used as found in the literature. In Tables 2 and 3 are reported the electrical and thermal properties of the two semiconductors [21,22], and the remaining generator parameters, respectively.

The tests were intended to have the same constant temperature on the bottom surface. However, due to the cooling system, using the ambient air as the sink, this constant value was not attained (32.7 ± 3.9 °C, Tables 4 and 5). The variation on the bottom surface, even if limited due to the efficient heat transfer between air and the circulating water, is mainly due to variation in the ambient temperature.

When comparing the experimental data with the results of the model, instead of a point to point comparison between data and predictions, a graphical comparison for groups of data (typically at the same power input or at the same resistance load) is adopted. To make this comparison clear, in the predictions a single reference temperature was chosen for the cold surface. This temperature is the average of those measured (32.7 °C, Tables 4 and 5).

Unlike typical data reductions which report voltage and power produced as a function of the circulating current ([6,11]), in this work particular emphasis is laid on the direct dependency of the parameters on the thermal quantities of the problem.

Table 2
Semiconductor properties referred to $T = 323$ K.

Semiconductors	Compound	α (μV K^{-1})	ρ (μ Ω m)	λ (W m^{-1}K^{-1})	Z (K^{-1})	References
p-type	$Bi_{0.5}Sb_{1.5}Te_3$	130	5.26	1.69	1.9×10^{-3}	[21]
n-type	Bi_2Te_3	−213	26.10	0.823	2.11×10^{-3}	[22]

Table 3
Thermophysical properties of the materials.

Data	Symbol	Value (W m^{-1} K^{-1})
Thermal conductivity of the ceramic plates [23]	λ_{cer}	36
Thermal conductivity of the cellular rubber [25]	λ_{ins}	$0.036 + 10^{-4}T$ (°C)
Thermal conductivity of the aluminium [26]	λ_{Al}	194
Thermal conductivity of the bolts [26]	λ_s	16
Thermal conductivity of the heater [26]	λ_{NiCr}	16

Table 4
Top and bottom experimental temperature for the open circuit condition.

Q_J	$R_1 = 11.14\ \Omega$				$R_2 = 22.39\ \Omega$				$R_3 = 39.20\ \Omega$				$R_4 = 86.22\ \Omega$			
	T_H	T_C	T_A	T_J	T_H	T_C	T_A	T_J	T_H	T_C	T_A	T_J	T_H	T_C	T_A	T_J
107.9	58.9	30.1	21.6	164.4	59.7	30.7	23.3	164.6	57.9	29.3	19.8	160.0	58.2	29.9	21.7	159.5
130.6	65.8	31.1	21.8	190.0	65.3	30.6	21.5	190.3	64.5	30.2	20.4	186.1	64.3	29.7	19.5	186.3
167.7	78.1	33.7	22.0	240.7	77.6	33.6	22.2	239.3	75.4	31.8	20.9	235.2	76.2	32.4	20.4	235.0
211.2	89.5	34.8	22.4	291.4	90.6	35.7	22.8	293.5	89.0	35.3	22.0	287.7	88.7	34.6	20.7	286.6
239.4	96.1	34.2	19.7	322.5	96.3	34.8	20.4	322.6	96.9	36.0	21.8	323.6	98.3	36.6	22.1	321.5

Table 5
Top and bottom experimental temperature for the closed circuit condition.

Q_J	R_1 = 11.14 Ω				R_2 = 22.39 Ω				R_3 = 39.20 Ω				R_4 = 86.22 Ω			
	T_H	T_C	T_A	T_J	T_H	T_C	T_A	T_J	T_H	T_C	T_A	T_J	T_H	T_C	T_A	T_J
108.4	55.0	30.1	21.6	162.0	56.3	30.2	22.7	163.3	55.1	28.9	21.1	158.2	56.6	29.4	21.4	159.5
130.5	60.0	30.0	21.2	186.6	61.5	30.6	21.5	188.3	61.4	29.9	20.8	185.0	62.1	29.5	19.7	184.4
167.1	71.7	33.5	22.9	236.8	72.3	33.2	21.7	236.9	71.1	31.5	20.3	231.5	73.5	31.8	21.1	234.0
210.4	81.5	34.1	21.8	288.4	83.8	34.9	22.7	290.7	83.6	34.5	22.1	284.8	85.2	34.2	21.4	283.9
240.7	87.1	33.5	19.4	320.1	89.1	34.2	19.9	321.4	91.6	35.1	21.3	322.6	94.4	36.0	21.6	320.1

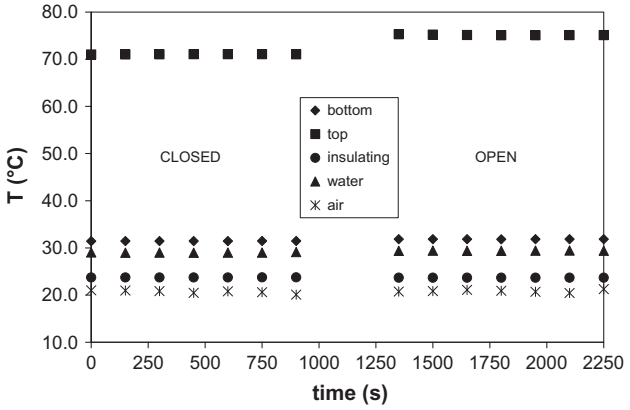

Fig. 6. Temperature distribution in a test (closed/open circuit).

The measurements are carried out for five values of the electric power supplied to the heater, Q_J; for each value of Q_J four different resistance loads are changed.

In Fig. 6 typical temperature distributions are shown for water, air, bottom and top surfaces of the modules and top surface of the insulating layer, for the cases of 'closed' and 'open' circuit, respectively. The two test cases are held at the same conditions. The temperature difference between the bottom and top surfaces of the modules is greater in the case of the 'open' circuit than for the 'closed' circuit. In both cases the bottom temperature is about 31 °C, while the top temperature is 71 °C and 75 °C, for the 'closed' and 'open' circuit, respectively.

In Tables 4 and 5 the temperatures are reported for the TEMs surfaces, heater top surface and air for the whole experimental set of trials. On the bottom surface the temperature is quite constant (32.7 ± 3.9 °C), while on the top the temperature varies from 55.0 °C to 98.3 °C. The spread of the top surface temperature depends on the heat power input supplied (Tables 6 and 7).

In Tables 4 and 5, for a given electric power supplied, Q_J, and different resistance loads, the top surface temperature of the Joule heater, T_J, does not change significantly. Since the heat leakage to the environment, Q_{env}, depends on T_J and on the ambient temperature, the heat power input into the thermoelectric generator, Q_{gen} in Eq. (14), seems to be independent of the resistance load.

In Tables 6 and 7 are summarized the values of Q_{gen} and Q_{TEM} obtained from the measured values of Q_J with the procedure described in Section 4. Since both the heat power input into the thermoelectric generator Q_{gen} and the temperature T_J seem to be independent of the resistance load, the two contributions, heat power input into the TEMs and heat lost through the assembly structures, seem to be also independent of the resistance load.

In Tables 8 and 9 are reported the different components of the heat flow balance, for the 'open' and 'closed' circuit, respectively. The heat losses through the stainless steel screws and through the thermal insulation between the TEMs (filling 2/3 of the total area of the generator) are both significant as it is the heat exchanged to the ambient.

The 'open' and 'closed' circuit voltage for the different resistance loads, grouped for different values of the heat flow into the TEMs (Tables 6 and 7) are shown in Fig. 7 as a function of the temperature. The 'open' circuit voltage increases as the temperature difference, ΔT, increases, and is well interpolated using a linear function. The same occurs for the 'closed' circuit voltage when considering a certain resistance load. These data also show other regular behaviour: for an assigned power input the temperature difference increases as the resistance load increases; if the resistance load

Table 6
Experimental data of the heat power input for the different data set (open circuit).

R_1 = 11.14 Ω			R_2 = 22.39 Ω			R_3 = 39.20 Ω			R_4 = 86.22 Ω		
Q_J	Q_{gen}	Q_{TEM}	Q_J	Q_{gen}	Q_{TEM}	Q_J	Q_{gen}	Q_{TEM}	Q_J	Q_{gen}	Q_{TEM}
107.9	101.8	81.0	108.6	102.6	81.6	107.4	101.5	80.7	107.6	101.8	80.9
130.5	123.1	97.8	131.0	123.5	98.2	129.4	122.1	97.0	131.4	124.1	98.6
167.9	157.3	124.8	167.9	157.4	124.9	167.8	157.5	125.1	167.1	156.8	124.5
211.3	196.7	155.9	212.0	197.3	156.4	211.2	196.9	156.1	210.5	196.3	155.6
237.3	219.7	174.1	238.9	221.3	175.3	240.1	222.5	176.2	241.3	224.0	177.4

Table 7
Experimental data of the heat power input for the different data set (closed circuit).

R_1 = 11.14 Ω			R_2 = 22.39 Ω			R_3 = 39.20 Ω			R_4 = 86.22 Ω		
Q_J	Q_{gen}	Q_{TEM}	Q_J	Q_{gen}	Q_{TEM}	Q_J	Q_{gen}	Q_{TEM}	Q_J	Q_{gen}	Q_{TEM}
107.8	101.9	81.0	109.5	103.6	82.4	108.0	102.3	81.4	108.5	102.7	81.7
130.7	123.4	98.1	130.4	123.0	97.8	130.2	123.0	97.8	130.8	123.6	98.2
166.2	155.9	123.8	168.2	157.8	125.3	165.8	155.7	123.7	168.2	158.0	125.4
212.0	197.7	156.8	212.3	197.9	156.9	208.8	194.8	154.4	208.7	194.8	154.5
239.0	221.7	175.8	240.8	223.4	177.1	242.9	225.4	178.6	240.3	223.0	176.7

Table 8
Components of the heat flow balance for the circuit closed on R_3.

Q_J (W)	Q_{env} (W)	Q_{ins} (W)	Q_b (W)	Q_{TEM} (W)
108.0	5.7	7.7	13.2	81.4
130.2	7.2	9.3	15.8	97.8
165.8	10.1	12.0	20.0	123.7
208.8	14.0	15.3	25.0	154.4
242.9	17.5	17.8	28.9	178.6

Table 9
Components of the heat flow balance for the open circuit.

Q_J (W)	Q_{env} (W)	Q_{ins} (W)	Q_b (W)	Q_{TEM} (W)
107.4	5.9	7.7	13.1	80.7
129.4	7.3	9.3	15.7	97.0
167.8	10.3	12.2	20.3	125.1
211.2	14.3	15.5	25.3	156.1
240.1	17.6	17.7	28.6	176.2

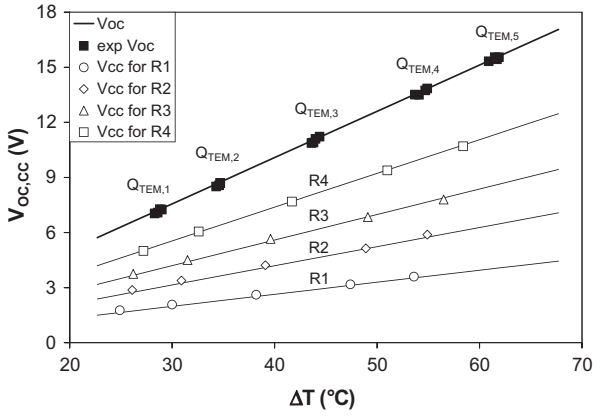

Fig. 7. Comparison between experimental and predicted data.

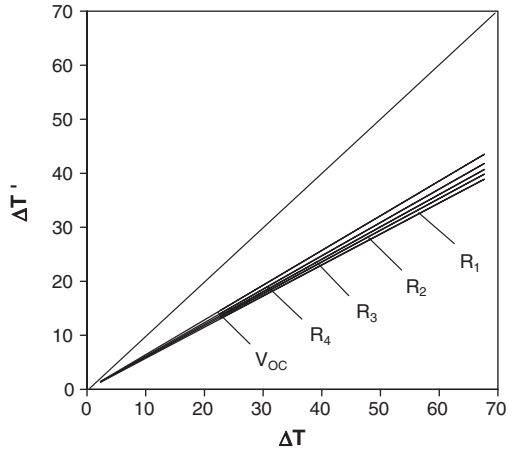

Fig. 8. Reduced temperature difference $\Delta T'$ versus ΔT and R_L.

becomes high, the 'closed' circuit voltage tends to the corresponding 'open' circuit voltage.

As previously emphasized, for each value of the heat flow into the TEMs, Q_{TEM}, the temperature difference, ΔT, between the bottom and the top of the modules increases as the resistance load increases (Fig. 7). This behaviour can be understood with the help of the theoretical model, by comparing the different contributions in Eq. (5). The Joule contribution is always smaller than those due to Peltier and Fourier and can be neglected. For the same heat power input into the modules, if the load resistance increases the circulating current decreases and thence the Peltier contribution decreases, whereas the Fourier contribution increases; therefore a higher temperature difference is experienced (see Appendix A for details).

Fig. 7 shows also the comparison between experimental and predicted data for the 'open' and 'closed' circuit voltage for different resistance loads. The comparison shows that the results given by the theoretical model are in very good agreement with the experimental data. The temperature difference, ΔT, is measured, on the bottom, on the assembly surfaces in the immediate proximity of the TEMs, and on the top, on the square plate of aluminium over the TEMs.

The temperature difference, $\Delta T'$, between the hot and cold junctions of the thermoelements is calculated from the temperature difference, ΔT, with the procedure explained in Section 3. Fig. 8 shows the trend of $\Delta T'$ versus ΔT. In the temperature range of the experiments a linear dependency is evident of $\Delta T'$ on ΔT for a fixed R_L; thus the predicted 'open' and 'closed' circuit voltage are linear functions of the temperature difference on the external surfaces of the modules, in agreement with the experimental evidence (see Appendix B for details).

Fig. 9 shows the theoretical and experimental power output. The data distribution is typical of a second order polynomial of the temperature difference, ΔT. The power output, P, obtained with the theoretical model is a second order function of the temperature difference, $\Delta T'$ (Eq. (4)); as previously observed there is an almost linear correlation between $\Delta T'$ and ΔT (Fig. 8); consequently, the predicted power output is a parabolic function of ΔT, in agreement with the experimental data (see Appendix B).

In Fig. 9, for the couples of resistance R_2 and R_3, R_1 and R_4 the power output shows quite overlapping trends; furthermore, the measured power output (Fig. 9) is greater for the resistance loads R_2 and R_3. This behaviour can be explained by Fig. 10, where the power output is plotted versus the resistance load. The different curves shown in Fig. 10 correspond to assigned values of thermal power input into the TEMs, Q_{TEM}. This is obtained as the average among the four experimental values pertinent to the five power inputs to the TEMs (Tables 7 and 8). The different curves shown in Fig. 10 have a maximum between R_2 and R_3. For the particular choice of the load resistances R_2 and R_3, the corresponding values of power output are quite equal. For the couple R_1 and R_4, a difference occurs. This difference increases when Q_{TEM} increases and can attributed to the different ΔT evident in Fig. 7 for a same Q_{TEM}, as discussed in Appendix A. The maximum power output is achieved for a load resistance of about 30 Ω, whereas the inner resistance is

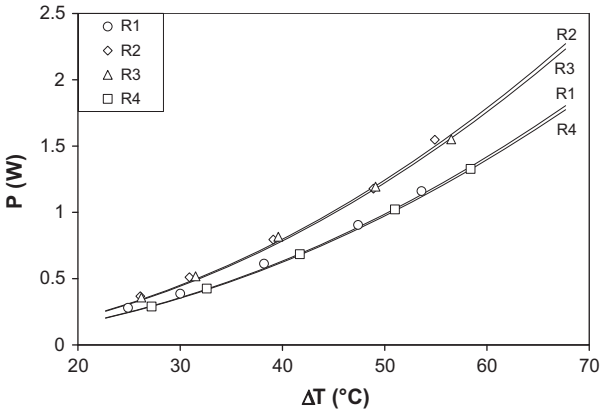

Fig. 9. Measured and calculated power output versus ΔT.

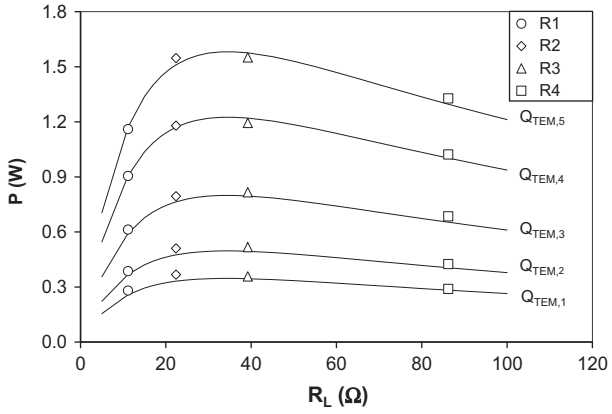

Fig. 10. Power output versus load resistance.

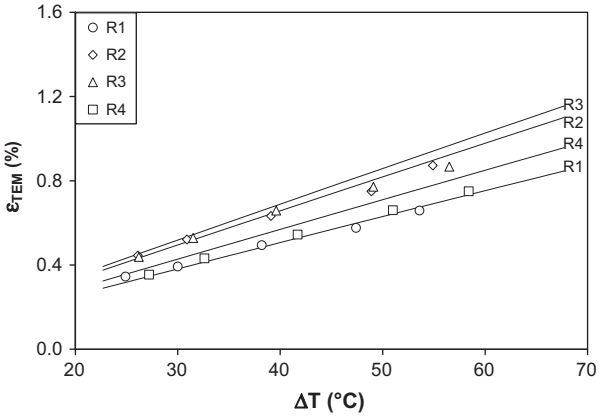

Fig. 12. Measured and calculated net efficiency versus ΔT.

27 Ω. This is in accordance with Freunek et al. [23] and implies that the load resistance enabling the generator to operate at the maximum output power is equal to the internal one added of a term function of $\Delta T'/\Delta T$.

The comparison of predictions and measurements based on electric power data (Figs. 7–10) is particularly good. When moving to the heat exchange, the accordance is no longer so good. In Fig. 11 the calculated heat power into the modules, Q_{TEM}, and into the generator, Q_{gen}, are compared with the corresponding experimental data. The agreement is good in terms of tendency, even if quantitatively poor. The calculated values are always lower than those measured. This difference is certainly due to a basic difficulty in assessing the thermal resistances in the experimental setup. Actually, these are calculated referring to the available schemes for the cooling of electronic systems [24] and seem to be lower than expected.

In Fig. 12 are shown the experimental values of the net efficiency of the TEMs, ε_{TEM}, as a function of the temperature. For each resistance load, the data distribution show a linear trend. In Fig. 12 are also shown the values of the net efficiency calculated by means of the theoretical model. The predicted values are higher than the experimental data (Fig. 12), this being in accordance with that previously observed. Referring to Eq. (16), for the power output (the numerator in Eq. (16)) in Fig. 9 there is a good agreement between theoretical and experimental data; for the heat flow (the denominator in Eq. (16)) in Fig. 11 the predictions are lower than the measurements. This makes the predicted efficiency higher than the measured one.

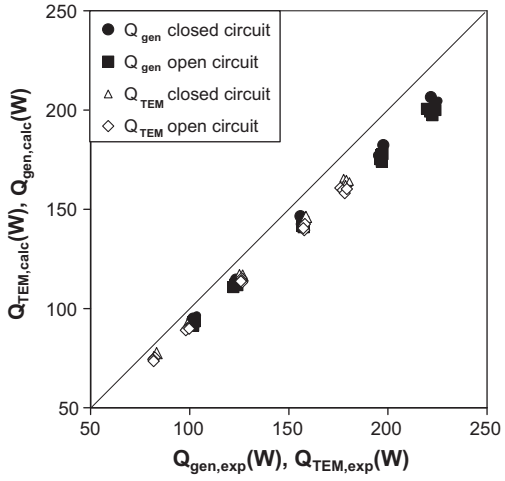

Fig. 11. Experimental and predicted power heat input.

Table 10
Experimental efficiency (%).

R_L = 11.14 Ω		R_L = 22.39 Ω		R_L = 39.20 Ω		R_L = 86.22 Ω	
$(\varepsilon)_{net}$	$(\varepsilon)_{ov}$	$(\varepsilon)_{net}$	$(\varepsilon)_{ov}$	$(\varepsilon)_{net}$	$(\varepsilon)_{ov}$	$(\varepsilon)_{net}$	$(\varepsilon)_{ov}$
0.35	0.27	0.45	0.35	0.44	0.35	0.36	0.28
0.39	0.31	0.52	0.41	0.53	0.42	0.43	0.34
0.49	0.39	0.63	0.50	0.66	0.52	0.55	0.43
0.58	0.46	0.75	0.60	0.77	0.61	0.66	0.52
0.66	0.52	0.87	0.69	0.87	0.69	0.75	0.59

In Table 10 are reported the net and the overall efficiency of the thermoelectric generator. The net efficiency does not exceed 1% while the overall efficiency reaches 0.7%. The lower overall efficiency is basically due to the presence of the thermal insulation among the modules. Furthermore, the measurement of the temperature on the hot side of the modules requires a thick layer of thermal grease between the top plate and the TEMs. This thick layer penalizes both the net and the overall efficiencies. Reducing this thickness in the model, the net efficiency increases to about 20% and the overall efficiency to about 25%.

In this work thermoelectric cooling modules (TECs) are used as thermoelectric generators (TEGs). In order to discuss this choice, TECs and TEGs are compared in terms of power output and conversion efficiency for the same condition (T_H = 90 °C and T_C = 30 °C). The thermoelectric modules are reversible and can be used both as TECs and as TEGs. However, different applications require specific arrangements.

In terms of themo-mechanical features, since the TEGs are submitted to higher temperature differences, the electrical wires are soldered on the cold side of the module and the insulating materials of the wires are rated for 250 °C. Since the TECs are submitted to higher circulating currents, the electrical wires of the TECs are thicker as their insulating materials, rated for 90 °C. Finally, the price of the TECs is sensibly lower than that of the TEGs [3].

In terms of thermo-electrical features, in Fig. 13 is shown a comparison of different commercial TECs and TEGs (Table 11) in terms of power output and overall conversion efficiency. The TEC used in this experiment gives performances sensibly lower than the other modules. The maximum power produced by the remaining modules is not so far and it is evident that in the present test conditions, if the quality of the semiconductors is high enough, a TEC can produce as a TEG. It can be concluded that TECs are an interesting alternative for power generation in the "low-heat" region [3]. Obviously, due to the thermo-mechanical features, if

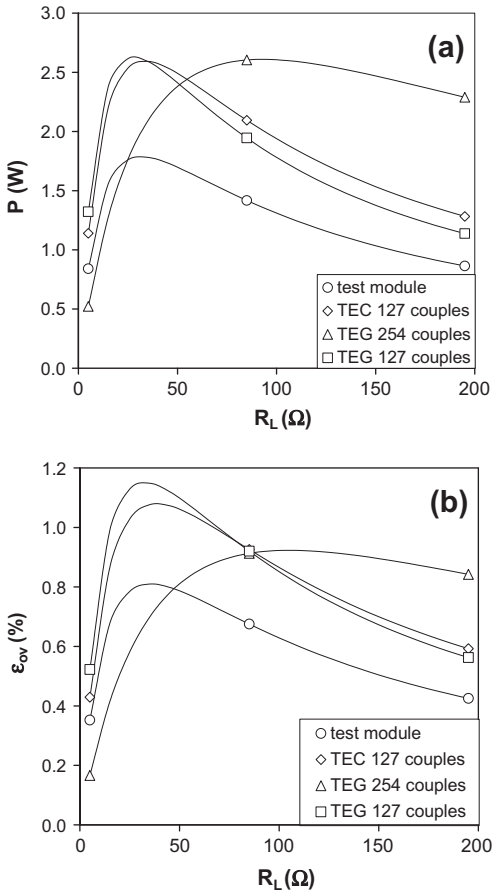

Fig. 13. Comparison of power output (a) and overall efficiency (b) for different TECs and TEGs in the same conditions (ΔT = 60 °C, T_C = 30 °C).

Table 11
Thermocouple properties for TEC and TEG module.

Module	N	Size (mm)	α (μV K^{-1})	K (mW K^{-1})	R (mΩ)	Z (K^{-1})
Test module	127	40 × 40 × 3.8	343	3.53	23.7	0.00141
TEC 127 couples	127	40 × 40 × 4.0	433	3.89	21.8	0.00210
TEG 254 couples	254	40 × 40 × 3.8	441	2.92	31.2	0.00213
TEG 127 couples	127	40 × 40 × 3.6	380	3.42	18.4	0.00229

higher temperature differences are available, TEGs become the right choice.

6. Concluding remarks

An experimental investigation has been carried out of the performance of multiple conventional Peltier devices used in the Seebeck mode as a thermoelectric generator. This was tested within a purpose-built heat transfer closed-loop.

The good agreement between the experimental and calculated values of the different parameters allows the use of the theoretical model as a tool of analysis of the generator performance. The low net efficiency is attributed to the heat transfer not being optimal and to the low quality of the modules. The commercial modules used in the experiment have a low figure of merit ($Z = 1.41 \times 10^{-3}$ K^{-1}), while for an efficient power generation higher values are preferred.

The comparison between the net and the overall efficiency highlights the negative role of the insulating layer and allows the reduction of the generator efficiency to be estimated.

This experimental work gives useful information to increase the effectiveness of devices for thermoelectric conversion.

It may be generally concluded that thermoelectric conversion is a promising way to the recovery of waste heat, because there is significant room for improvement: the use of suitable modules for the Seebeck mode, a greater care of the thermal contact with the hot and the cold source and a greater density of the modules in the generator. Furthermore, the conversion efficiency reached in the range of the temperature difference of the experiment is rather low, so the trend of the gathered data allows the behaviour of a generator with higher heat power input to be predicted.

Acknowledgements

The authors are grateful to C. Soffritti and M. Merlin for the measurements and the X-ray spectroscopy analysis carried out on the thermoelements.

Appendix A

Eq. (5) can be simplified neglecting the thermal resistance of the ceramic plates and the Joule contribution, always very small. Then Eq. (5) can be rewritten as:

$$Q_{\mathrm{TEM}} = mN\left[K'\left(T'_H - T'_C\right) + (\alpha_p - \alpha_n)T'_H I\right] \tag{A.1}$$

Eq. (A.1) can be rewritten to put in evidence the contribution due to T'_H:

$$\frac{Q_{\mathrm{TEM}}}{mN} + K'T'_C = \left[K' + I(\alpha_p - \alpha_n)\right]T'_H \tag{A.2}$$

Since the bottom temperature T_C is quite constant (Tables 5 and 6) and the thermal conductance K_C is very high, the temperature T'_C is also quite constant, as is Q_{TEM} (Tables 7 and 8). Thence, the left term of Eq. (A.2) is constant and when the circulating current I increases the temperature T'_H decreases.

Appendix B

In Fig. 8 is shown the temperature difference on the junctions, $\Delta T'$, as a function of that outside the ceramic plates, ΔT, and of the resistance load, R_L. The dependency is linear and in first approximation, can be expressed as:

$$\Delta T' = C(R_L)\Delta T \tag{B.1}$$

where the constant C is a function of R_L. Consequently, Eqs. (2), (4), and (8) can be expressed as a function of ΔT. For example the 'closed' circuit voltage becomes:

$$V_{\mathrm{CC}} = \frac{R_L}{(R_{\mathrm{TEM}} + R_L)} mN(\alpha_p - \alpha_n)C(R_L)\Delta T \tag{B.2}$$

References

[1] D.M. Rowe, Miniature semiconductor thermoelectric devices, in: D.M. Rowe (Ed.), Handbook of Thermoelectric, CRC Press, Boca Raton, 1995, pp. 441–458.
[2] S.A. Omer, D.G. Infield, Design optimization of thermoelectric device for solar power generation, Solar Energy Materials and Solar Cells 53 (1998) 67–82.
[3] S. Maneewan, S. Chindaruksa, Thermoelectric power generation system using waste heat from biomass drying, Journal of Electronic Materials 38 (2009) 974–980.
[4] S.B. Riffat, X. Ma, Thermoelectrics: a review of present and potential applications, Applied Thermal Engineering 23 (2003) 913–935.
[5] L.E. Bell, Colling, heating, generating power, and recovering waste heat with thermoelectric systems, Science 321 (2008) 1457–1461.
[6] T. Kajikawa, Approach to the practical use of thermoelectric power generation, Journal of Electronic Materials 38 (2009) 1083–1088.
[7] J. Vázquez, M.A. Sanz-Bobi, R. Palacios, A. Arenas, State of the art of thermoelectric generator based on heat recovered from the exhaust gases of automobiles, in: 6th Eur. Conf. on Thermoelectr., July 2–4, Paris, France, 2008.

[8] F.A. Leavitt, N.B. Elsner, J.C. Bass, Use application and testing of the HZ-14 thermoelectric module, in: 15th Int. Conf. on Thermoelectr., 1996.
[9] H. Takazawa, H. Obara, Y. Okada, K. Kobayashi, T. Onishi, T. Kajikawa, Efficiency measurement of thermoelectric modules operating in the temperature difference of up to 550 K, in: 25th Int. Conf. on Thermoelectr., 2006.
[10] L. Rauscher, S. Fujimoto, H.T. Kaibe, S. Sano, Efficiency determination and general characterization of thermoelectric generators using an absolute measurement of the heat flow, Measurement Science and Technology 16 (2005) 1054–1060.
[11] E. Sandoz-Rosado, R.J. Stevens, Experimental characterization of thermoelectric modules and comparison with theoretical models for power generation, Journal of Electronic Materials 38 (2009) 1239–1244.
[12] X. Gou, H. Xiao, S. Yang, Modelling, experimental study and optimization on low-temperature waste heat thermoelectric generator system, Applied Energy 87 (2010) 3131–3136.
[13] D.T. Crane, G.S. Jackson, Optimization of cross flow heat exchangers for thermoelectric waste heat recovery, Energy Conversion and Management 45 (2004) 1565–1582.
[14] K.M. Saqr, M.K. Mansour, M.N. Musa, Thermal design of automobile exhaust based thermoelectric generators: objectives and challenges, International Journal of Automotive Technology 9 (2008) 155–160.
[15] X. Niu, J. Yu, S. Wang, Experimental study on low-temperature waste heat thermoelectric generator, Journal of Power Sources 188 (2009) 621–626.
[16] Z. Luo, A simple method to estimate the physical characteristic of a thermoelectric cooler from vendor datasheet, Electronics Cooling 14 (3) (2008) 22–27.
[17] R. Palacios, A. Arenas, R.R. Pecharromán, F.L. Pagola, Analytical procedure to obtain internal parameter from performance curves of commercial thermoelectric modules, Applied Thermal Engineering 29 (2009) 3501–3505.
[18] G.L. Morini, Analytical determination of the temperature distribution and Nusselt numbers in rectangular ducts with constant axial heat flux, International Journal of Heat and Mass Transfer 43 (2000) 741–755.
[19] M. Chen, S. Lu, B. Liao, On figure of merit thermoelectric generators, Journal of Energy Resource Technology 127 (2005) 37–41.
[20] D.M. Rowe, Gao Min, Peltier devices as generators, in: D.M. Rowe (Ed.), Handbook of Thermoelectric, CRC Press, Boca Raton, 1995, pp. 479–488.
[21] J. Navrátil, Z. Starý, T. Plecháček, Thermoelectric properties of p-type antimony bismuth telluride alloys prepared by cold pressing, Materials Research Bulletin 31 (1996) 1559–1566.
[22] G.J. Snyder, Thermoelectric power generation: efficiency and compatibility, in: D.M. Rowe (Ed.), Thermoelectric Handbook Macro to Nano, vol. 9, CRC Press, Boca Raton, 2005, pp. 1–26.
[23] M. Freunek, M. Müller, T. Ungan, W. Walker, L.M. Reindl, New physical model for thermoelectric generators, Journal of Electronic Materials 38 (2009) 1214–1220.
[24] Y.A. Çengel, Heat Transfer: A Practical Approach, second ed., McGraw Hill, New York, 2003.
[25] Armacell GmbH, Technical data AF/Armaflex2007INT.pdf.
[26] J.H. Lienhard, A Heat Transfer Textbook, third ed., Phlogiston Press, Cambridge, Massachusetts, 2006.